Preprint typeset in JINST style - HYPER VERSION

Passive 3D Imaging of Nuclear Waste Containers with Muon Scattering Tomography

C. Thomay[a]*, J. Velthuis[a], T. Poffley[a], P. Baesso[a], D. Cussans[a], L. Frazão[a]

[a] *University of Bristol,*
H. H. Wills Physics Laboratory, Tyndall Avenue, Bristol
BS8 1TL, United Kingdom
E-mail: christian.thomay@bristol.ac.uk

ABSTRACT: The non-invasive imaging of dense objects is of particular interest in the context of nuclear waste management, where it is important to know the contents of waste containers without opening them. Using Muon Scattering Tomography (MST), it is possible to obtain a detailed 3D image of the contents of a waste container on reasonable timescales, showing both the high and low density materials inside. We show the performance of such a method on a Monte Carlo simulation of a dummy waste drum object containing objects of different shapes and materials. The simulation has been tuned with our MST prototype detector performance. In particular, we show that both a tungsten penny of 2 cm radius and 1 cm thickness, and a uranium sheet of 0.5 cm thickness can be clearly identified. We also show the performance of a novel edge finding technique, by which the edges of embedded objects can be identified more precisely than by solely using the imaging method.

KEYWORDS: Search for radioactive and fissile materials; Analysis and statistical methods; Particle tracking detectors (Gaseous detectors).

*Corresponding author.

Contents

1. Introduction

In the context of legacy nuclear waste management, non-invasive imaging is of particular interest. In the operation of nuclear power plants, materials become irradiated, and radioactive waste, which includes nuclear fuel and cladding, accumulates. Radiation hazards from these types of materials can be significant[1], which makes safe handling and storage imperative. Safe long-term storage of this nuclear waste is a matter of ongoing active discussion, and no universally satisfactory solution has yet been found; geological disposal has become a widely accepted option, but there are many technical issues in moving from storage to disposal[2]. In the meantime, nuclear waste is generally stored in intermediate storage facilities where, dependent on the amount of irradiation or radioactivity of the waste at hand, storage vessels of various shapes and sizes are used. Often these vessels come in the form of waste drums: steel containers where the waste is filled in concrete.

For safety reasons, it is of interest to know the material content of these drums. Even though in principle it should be known what was stored in which vessel, individual vessels may date back a long time, and both physical and chemical processes inside may have affected and altered the composition of the waste. In particular, uranium corrosion can lead to the build-up of gas, which results in expansion of the vessels and could cause them to crack or even rupture. Once sealed, it is not desirable to open the vessels again, in particular because of the aforementioned effects which could have dangerous consequences if the vessels were opened carelessly. Consequently, non-invasive imaging methods are of prime interest, and cosmic muons are excellent probes for this purpose, since they are part of the natural background radiation (so no additional radiation is introduced), and their strong penetrative power makes them well-suited to gain information about the content of dense objects.

Muon Scattering Tomography (MST) uses the scattering behaviour of cosmic muons within the object of interest in order to obtain an estimate of the material content within. MST began with the work of the group at LANL[3], with the intent of scanning trucks and cargo containers to detect illicitly transported special nuclear material.

Our group in Bristol has developed RPCs (resistive plate chambers) for MST in collaboration with AWE in the context of national safeguards. For that purpose, a small-scale prototype consisting of 12 RPCs with a fiducial region of 48 x 48 cm^2 was developed, and after the successful completion of this system, a large-scale prototype consisting of 24 RPCs with a fiducial region of 178 x 54 cm^2 was built. Details and results of both systems can be found in [4, 5]. The simulated detectors used in this study have been based on these detectors; in particular, the intrinsic spatial resolution was assumed to be 450 μm based on the prototype results.

In MST, the muon trajectories above and below the inspection volume are measured, and the volume is divided into sub-volumes. From the scattering inside these sub-volumes, discriminating values can be calculated that are indicative of the material within. From these values, a 3D image can be generated. The most commonly used 3D reconstruction method in literature is the EM method[6], which uses an expectation-maximization algorithm to calculate the most likely scattering lengths inside the volume. The method provides a 3D image of the scanned object, however it has been reported to require computing time comparable to the data taking time[6]. This method has recently been applied to the study of encapsulated nuclear waste[7].

2. Muon Scattering Tomography

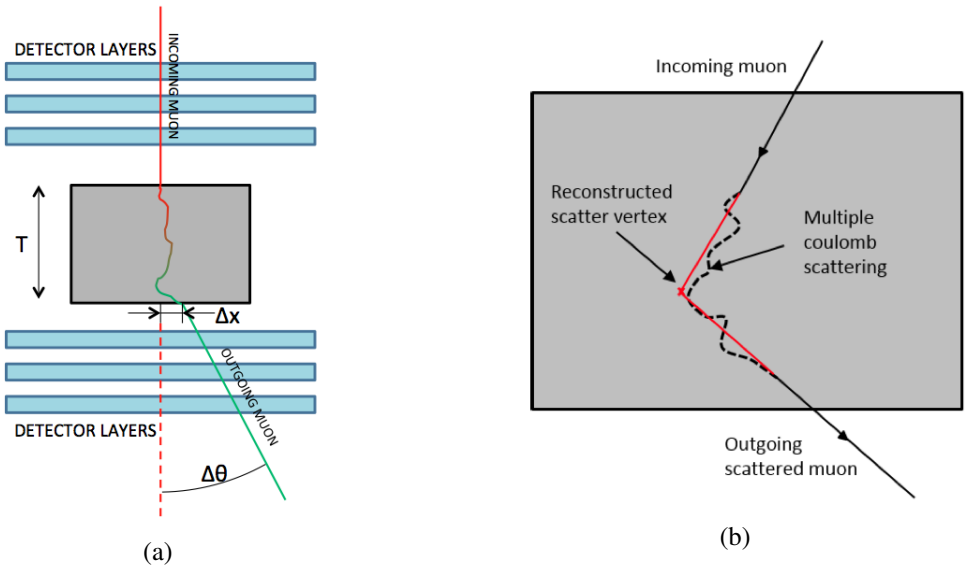

Figure 1: (a) Muon scattering principle: 3 detector layers respectively measure the muon track above and below the volume of interest. (b) Illustration of vertex principle.

Muons undergo multiple Coulomb scattering when traversing matter (see fig. 1a). The distri-

bution of projected scattering angles is approximately Gaussian, with the width σ given by[8]

$$\sigma = \frac{13.6\,\text{MeV}}{pc\beta} z\sqrt{X/X_0}(1+0.038\ln(X/X_0)), \tag{2.1}$$

$$X_0 = \frac{A \cdot 716.4\text{g/cm}^2}{Z(Z+1)\ln(287/\sqrt{Z})} \tag{2.2}$$

for a muon with momentum p, velocity βc, and charge number z in a material of thickness X, mass number A and atomic number Z. We assume that the incoming and outgoing tracks scatter in one location (the vertex). This is a useful approximation giving a roughly correct localization of the muon scattering (especially for scattering in high-Z materials), despite the fact that the muon undergoes many small scatters when traversing matter (see fig. 1b).

Track and vertex fitting is performed in one step, by fitting the 3 vertex position coordinates and the 4 track slopes (for the incoming and outgoing track in x and y) to the hit position data points from the detector. This is done by defining a minimization function E:

$$E = E_x + E_y, \tag{2.3}$$

$$E_x = \sum_{i=1}^{3} \frac{(h_i - (v_x + k_{\text{x,upper}} \cdot t))^2}{\sigma_{h_i}^2} + \sum_{i=4}^{6} \frac{(h_i - (v_x + k_{\text{x,lower}} \cdot t))^2}{\sigma_{h_i}^2}, \tag{2.4}$$

$$\text{with } t = z_i - v_z \tag{2.5}$$

and h_i the measured hit positions, z_i the positions in the z-plane (i.e. the known detector positions), v_x, v_y, v_z the scatter vertex positions, k the track parameters, and σ_{h_i} the measurement errors on the hit positions. E_y is defined analogously. The axes are defined such that the RPCs are flat in the (x,y)-plane. Minimization is performed in ROOT[10] using the Minuit package[11].

The muon momentum is an important additional ingredient due to the dependency of eq. (2.1) on p. An estimate of the momentum can be obtained from the scattering within the detector layers. For such a system, a momentum resolution of about 50% can be achieved[12], so a momentum error of 50% was assumed.

3. Imaging Method

The method takes a similar approach as [13]. The imaging algorithm subdivides the volume under consideration into cubic bins. In contrast to the application in [13], however, scanning time is not of the essence, but detecting small objects is; therefore small bins of no more than 1 cm side length are used for this application. In each bin, the set of muon tracks whose vertex is located in the bin is considered, and for each pair i, j of these muon tracks, a weighted metric value is calculated:

$$\widetilde{m}_{ij} = \frac{\|\mathbf{v_i} - \mathbf{v_j}\|}{(\theta_i p_i) \cdot (\theta_j p_j)}, \tag{3.1}$$

where $\mathbf{v_i}$ is the vertex position of muon i, θ_i the scatter angle, and p_i the momentum. The 'true' momentum from the simulation is used in this calculation with an error of 50%: a Gaussian spread with a width of 50% of the true value has been added to each momentum value.

The natural logarithm of the weighted metric is taken in order to condense the range of the values. Figure 2 shows distributions of these values for different materials. As the discriminator d, the median of this distribution is extracted for every bin. The distribution of the metric values is, for a fixed exposure time and bin geometry, dependent on the material content. The same material yields a different discriminator if the number of muons going through the volume is different. For that reason, a fixed number of muons is considered for every bin; this ensures that the discriminator values from different bins can be compared.

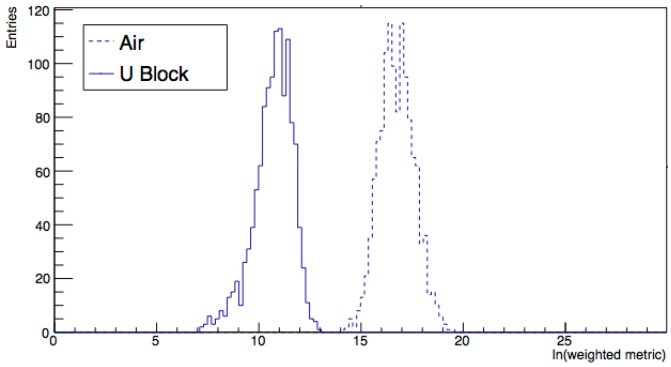

Figure 2: Distribution of the logarithm of the weighted metric for 1 minute of muons passing through a volume containing air, and a 10 cm side length U cube (MC simulation, using the setup as described in section 4). The scattering in the U cube shifts the distribution to lower values.

4. Simulation Results

In order to evaluate the imaging method, a Geant4[14] simulation based on the 12-layer prototype system described in [4] was used. The simulated system consists of 12 layers of RPCs with one-dimensional readout and a fiducial region of 100 x 100 cm^2 each. 6 RPCs each are placed above and below an inspection volume. The spacing between two RPCs in the same direction is 90 mm. An intrinsic spatial resolution of 450 µm for the detectors was assumed. Cosmic muons were simulated with CRY[15].

A standard intermediate level waste (ILW) drum has a volume of 500 litres[16], with a maximal height of 123 cm and a maximal diameter of 80 cm. In order to test the imaging methods, a smaller waste drum of about 26 litres was considered; this type of waste drum is planned to be investigated with the laboratory RPC detector setup in the future.

Due to the diversity of the materials that could be encountered in nuclear waste, an 'example' scenario was simulated. The cylindrical steel drum (diameter 26 cm, length 50 cm, with a steel flange at the top) is filled with concrete and contains dummy objects: a cylindrical U rod (1 cm radius, 10 cm height), a thin quadratic U sheet (0.5 x 10 x 10 cm^3), three W pennies of 1 cm thickness (1 cm, 2 cm, and 4 cm radius), and a cylindrical air enclosure with 5 cm thickness and 10 cm radius (see fig. 3). This cylinder was placed 'flat', i.e. with the cylinder axis along x parallel to the RPCs, in the inspection volume between the two sets of RPCs. All results presented in this and the following sections were obtained using this detector setup.

The results presented in this section were obtained using a muon flux equivalent to 2 weeks of data-taking, using bins of 1 cm side length. A particular advantage of this analysis method is that the reconstruction time is very short: 2 weeks of data take less than an hour to process on a desktop computer.

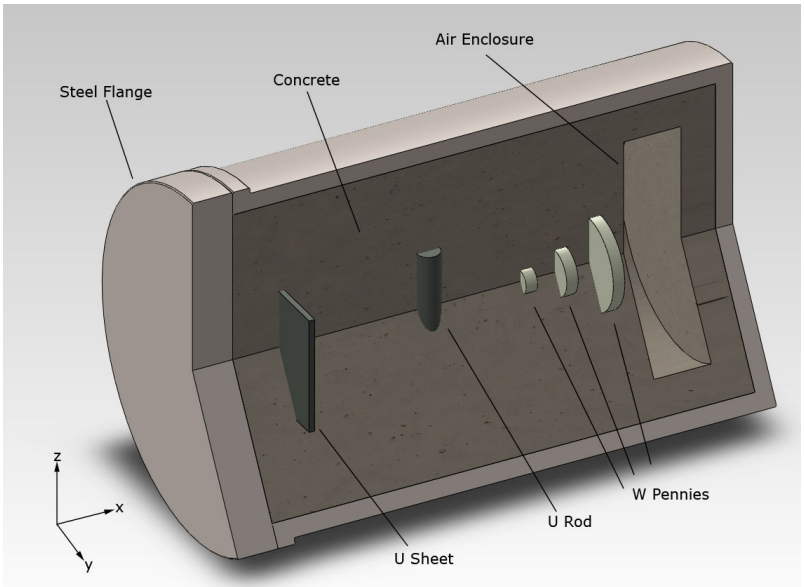

Figure 3: Simulated waste drum schematic.

Due to the fact that detectors are used above and below the target in z, the vertex position will be precise in the x- and y-plane, but fairly uncertain in the z-plane (illustrated in fig. 4a). In order to counteract this, the drum was scanned in 4 different rotations around the x-axis (0°, 90°, 180°, and 270°) during the total data-taking period of 2 weeks, and the results were combined.

Figure 4b shows metric discriminator values for bins containing only uranium, and bins containing only concrete. It can be seen that the two distributions are clearly separated. Based on this, a discriminator threshold value of 8.8 was chosen in order to remove the concrete background.

Figure 5 shows a 3D image of the entire waste drum. The concrete is visible as light yellow, and denser objects are visible towards the red end of the spectrum. The air enclosure is transparent / light blue. Except for the 1 cm W penny, all objects can be clearly seen in the 3D representation.

Figure 6 shows 2D slices in x of 1 cm thickness, containing some of the enclosed objects, where only bins below threshold are shown to remove the concrete background. The grid position was not chosen to line up with the object boundaries in x; the true positions of the W pennies, due to their thickness of 1 cm, are partially contained in two neighbouring slices. The uranium sheet, due to its thickness of 0.5 cm, is completely contained in one slice.

The shapes of the uranium sheet and the 4 cm tungsten penny are very clear. The 2 cm penny is also visible, and indicative signal of the 1 cm tungsten pennies can be seen. As an indicator of object identification, an inclusion percentage value was added, defined in the x-slice as the ratio of the bins below cut included in the known shape of the object divided by the total number of bins below cut. It can be seen that all but the smallest tungsten penny are identified well: the uranium

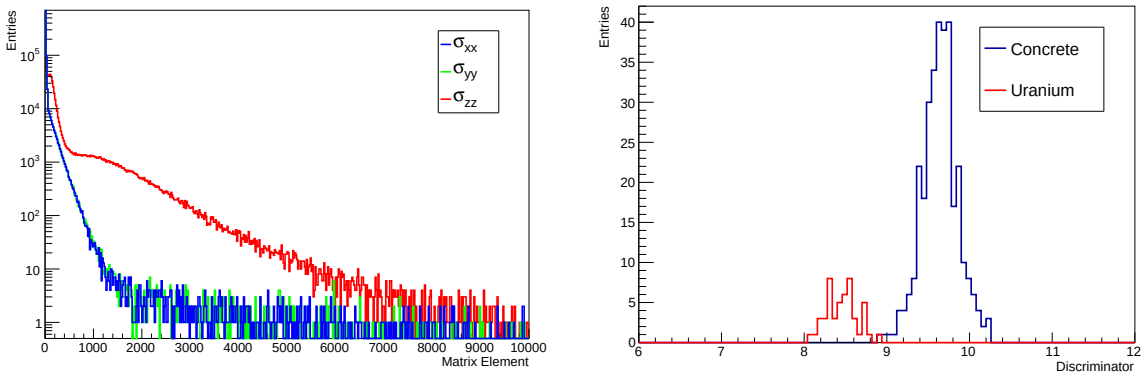

(a) (b)

Figure 4: (a) Comparison of scattering vertex covariance matrix elements. The RPCs are in the (x,y)-plane. The uncertainty is significantly larger along the z-axis, orthogonal to the detectors. (b) Distributions of metric method discriminator values from bins containing uranium, and bins containing only concrete.

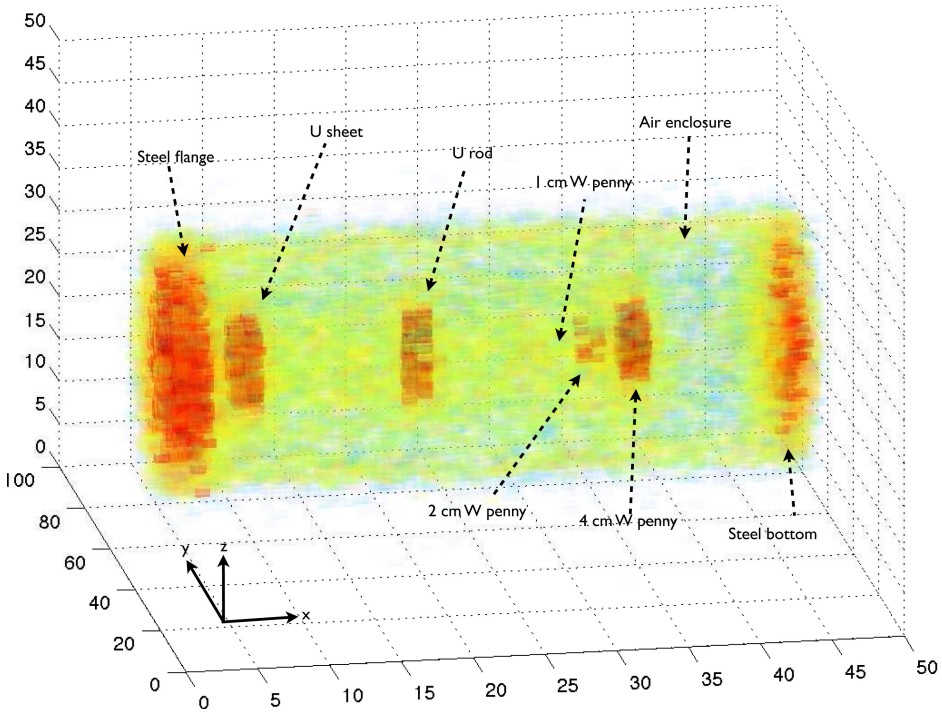

Figure 5: Waste drum 3D image. The concrete is visible as light yellow, and denser objects are visible towards the red end of the spectrum. The air enclosure is visible as blue. All axes are in cm.

sheet has an inclusion percentage of 86%, so 86% of all bins below threshold are contained in the shape of the sheet. The 4 cm tungsten penny is similarly well resolved with an inclusion percentage of 85%. The limit of precision can be seen for the smallest penny: while the 2 cm penny is still

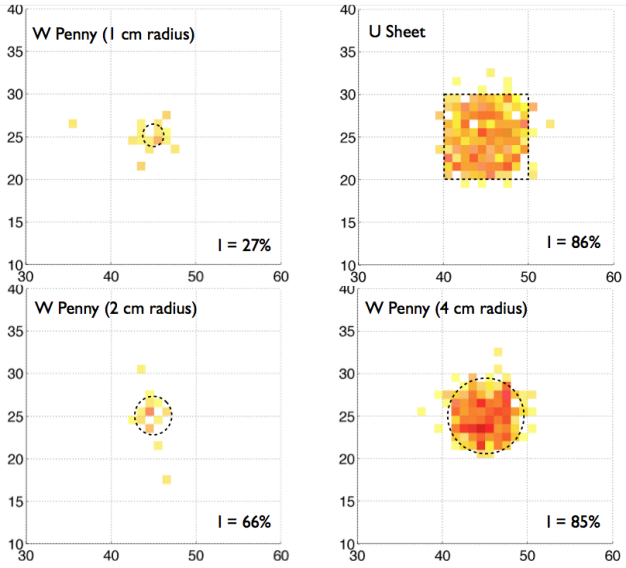

Figure 6: 2D slices with different objects in the waste drum. Clockwise from top right: U sheet, 4 cm W penny, 2 cm W penny, and 1 cm W penny. 'True' shapes outlined and inclusion percentages added. All axes are in cm.

visible and fairly well-defined at 66%, for the 1 cm penny most of the bins below threshold are outside the shape of the penny, resulting in an inclusion percentage of 27%.

5. Edge Finding

The shapes of the objects in figure 6 can, to an extent, be made out by eye. However, at this stage the edges of the objects are, at best, as precise as the binning of the volume of interest. In order to make the shape reconstruction more precise, an edge finding method was implemented, with the aim of identifying more precisely where an embedded objects begins and ends.

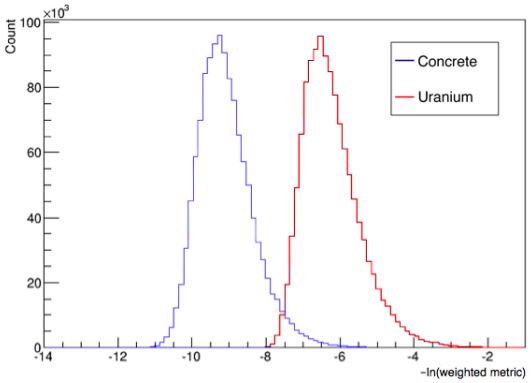

Figure 7: Distribution of the negative logarithm of weighted metric values for bins containing uranium, and bins containing concrete.

The edge finding is based on the fact that, if the bin under consideration is on the edge of an embedded object, i.e. containing both concrete and the object in question, a mixing effect will occur in the metric distribution. The metric distributions for single materials have a shape similar to a Landau distribution when the negative logarithm of the weighted metric values are used (i.e. $-\ln(\widetilde{m}_{ij})$ instead of $\ln(\widetilde{m}_{ij})$ from eq. (3.1), see fig. 7). Consequently, the mixing effect can be approximated with a fit of the sum of two Landau distributions,

$$\begin{aligned} F = \; & A_1 \exp\left(-\tfrac{1}{2}\left(\tfrac{x-\mu_1}{\sigma_1}\right) + \exp\left(\tfrac{x-\mu_1}{\sigma_1}\right)\right) \\ & + A_2 \exp\left(-\tfrac{1}{2}\left(\tfrac{x-\mu_2}{\sigma_2}\right) + \exp\left(\tfrac{x-\mu_2}{\sigma_2}\right)\right). \end{aligned} \tag{5.1}$$

The values for μ_1, μ_2, σ_1 and σ_2 are taken from fits of single Landau distributions to bins in areas with only concrete or only uranium far away from any material interface. Therefore, the double Landau fit only has two free parameters: the amplitudes of each of the Landau distributions, A_1 and A_2.

The mixing effect, together with the double Landau fit, can be seen in figure 8a. In order to enhance the visibility, figures 7 and 8a show the distributions for a large number of bins with the respective materials.

From the double Landau fit, a new discriminator d_{Landau} is calculated as a ratio of the amplitudes of the two Landau distributions:

$$d_{\text{Landau}} = \frac{A_2 - A_1}{A_2 + A_1}. \tag{5.2}$$

By definition, d_{Landau} is in the range of [-1, 1], taking a value of -1 if only material 1 is present, and a value of 1 if only material 2 is present. As such, d_{Landau} reflects the mixing of the two materials in the bin under consideration. For instance, the fit in figure 8a results in a d_{Landau} close to 0.

The edge finding method uses d_{Landau} by repeating the analysis multiple times, each time shifting the grid by a small amount in a set direction. Consequently, in the bins on the edge of the object of interest, the mixing will gradually increase, until the discriminator is fully dominated by one material. The edge of the object is defined as the position where d_{Landau} exceeds 0.99.

As an initial test, the edge finding has been applied to simulated data sets with the waste drum described above, each containing a 10 x 10 x 10 cm^3 cube of different materials. In terms of rotation, the cube was aligned with the axes of the coordinate system. 25 days of cosmic muon exposure were used, with a bin size of 7 mm. The grid was shifted by 1 mm in each step, resulting in 7 iterations of the algorithm; each iteration requires less than 1 hour of computing time. The result for a cube of uranium can be seen in figure 8b, where d_{Landau} is shown for a scan along the y axis through the U cube. The position where the edges were found are marked with a red line. It can be seen that the side length of the cube is reconstructed close to the correct value of 10 cm.

The size scan as shown in figure 8b was performed along the y axis at a fixed position in x and z, and yields one measurement of the size of the object along this axis. Since the object in question is a cube, the scan can be repeated on the same data set at different positions in x and z; since the length of the cube is the same, these scans can be considered measurements of the same length. From the spread of these measured size values, the resolution of the method in measuring the size of an object of this size and composition can be calculated.

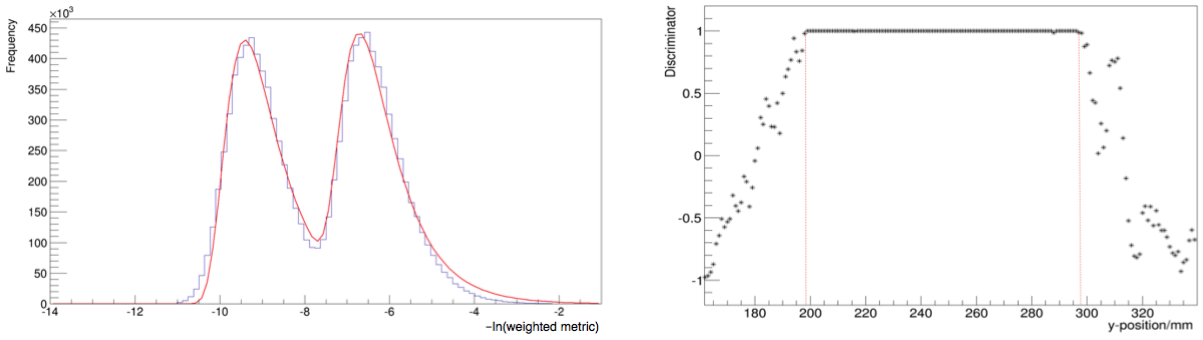

(a) (b)

Figure 8: (a) Double Landau fit applied to multiple bins containing both uranium and concrete. The overlap between the two distributions is due to the mixing effect. (b) Edge finding scan along y with double Landau fit. Each entry corresponds to the value of the discriminator at the respective bin center, combining the data from all shifted grids.

This size resolution σ was calculated as

$$\sigma = \sqrt{\frac{\sum_i (l_t - l_{r,i})^2}{n}}, \tag{5.3}$$

where l_t is the true simulated size, $l_{r,i}$ the reconstructed sizes, and n the number of estimates of the cube size. This way, a resolution of $\sigma = 2.1 \pm 0.5$ mm was found for the uranium cube of 10 cm side length. This was repeated for cubes made of tungsten, lead, and iron; the results are summarised in table 1.

Material	Density (g/cm^3)	Radiation Length (cm)	Resolution (mm)
Uranium	19.0	0.316	2.1 ± 0.5
Tungsten	19.3	0.35	2.3 ± 0.6
Lead	11.4	0.56	2.6 ± 0.6
Iron	7.87	1.76	3.4 ± 0.7

Table 1: Resolution results, calculated using eq. (5.3), from double Landau fit for 10 cm cubes of different materials, using 25 days of data. Material constants from [9].

The dependence of the size resolution on the exposure time was also investigated. The waste drum with the 10 cm uranium cube was scanned for time periods between 6.25 days to 50 days. The resulting resolution results can be seen in figure 9. As is to be expected, the resolution decreases with increasing scan time, with the improvement beginning to level off after 30 days.

Finally, the scan was performed for simulations of the waste drum with uranium sheets of 0.5 cm thickness and different side lengths, using 32 days of muon exposure. The simulated size versus the reconstructed size can be seen in figure 10 for sheets with side lengths between 4 and 10 cm. It can be seen that regardless of the sheet size, the reconstructed size is very close to the simulated size. A straight line fit has been performed through the data points, with the fit parameters

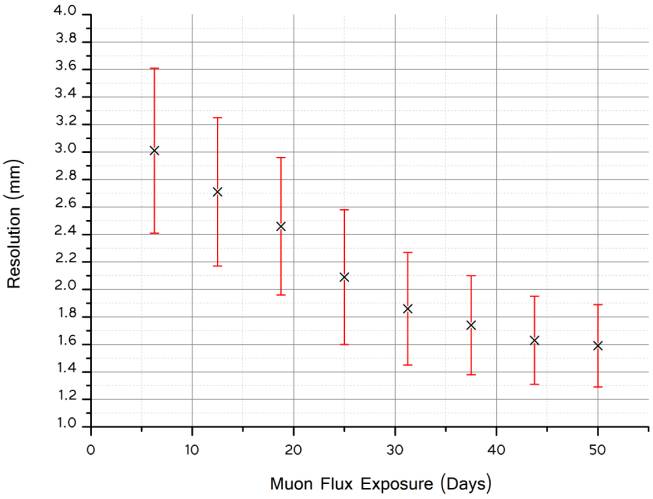

Figure 9: Resolution values for the reconstruction of a 10 cm uranium cube using a bin size of 7 mm for various muon flux exposures.

shown in fig. 10. The fit is in good agreement with an intercept of 0 ($p_0 = 1.16 \pm 3.85$) and a slope of 1 ($p_1 = 0.98 \pm 0.05$).

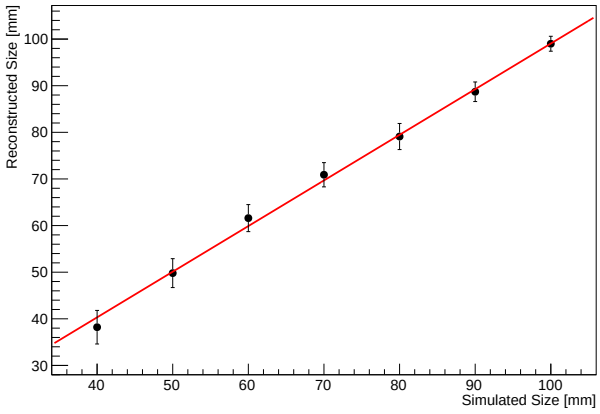

Figure 10: Reconstructed size versus simulated size for U sheets with 0.5 cm thickness, using 32 days of data.

Each of the data points in figure 10 shows the respective average reconstructed size, with the corresponding size resolution as the error bars. The spread of these values from the true sizes can now be interpreted as an overall size resolution of the method, for sheets between 4 cm and 10 cm side length. The overall resolution obtained this way is $\sigma = 1.20 \pm 0.37$ mm, which now applies to a wider range of object sizes.

6. Discussion

In the previous sections, we have shown that the metric method can be used to obtain 3D images of dense objects. However, existing methods in the field, in particular the EM algorithm[6], have been used in the past for the same purpose. The EM algorithm contains a more precise modelling of the underlying physical process, at the cost of higher computational complexity. While it is advantageous to some extent that the metric method is faster, when considering the data taking times necessary to imagine nuclear waste using MST, this advantage seems less significant.

However, this is where the other advantage of our method comes into play, which is the edge finding using shifted grids. This approach allows us to identify object sizes with a precision greater than what could be achieved with the voxel grid alone. While a similar approach could also be implemented using the EM algorithm, the short runtime of our method makes the repeated analysis on shifted grids a feasible approach, whereas it is uncertain whether the same could be said for the EM algorithm.

In terms of computing time, if the edge scan is repeated along every axis, the object boundaries can be completely identified in $3 \times n_{\text{steps}}$ iterations, so for e.g. steps of 1 mm and 7 mm bin size, 21 total iterations are necessary; with less than an hour per iteration, this puts the total computing time for a complete edge scan at less than a day. Since the shifts are independent from one another, each iteration could also be computed in parallel.

An important aspect to note is that the performance of the edge finding does not require the objects to be favourably aligned with the grid, since the mixing effect will gradually increase as the bins are shifted into the object shape, regardless of where the object lies in regard to the grid. Furthermore, knowledge of the true position of the objects is not necessary: from a scan such as in fig. 8b, the position of the object on that particular line through the volume of interest can be inferred without prior knowledge of the object position. From scans along all lines in the volume of interest in x-, y-, and z-direction, the entire object shape can be reconstructed. In a real life usage, estimated shapes of objects inside the concrete could be obtained this way. The precise edge finding has a particular usefulness in the search for uranium corrosion, where it is of interest to identify and monitor minor changes in the size of embedded uranium objects.

7. Conclusion & Outlook

We have shown the performance of a method using the scattering behaviour of cosmic muons to image nuclear waste drums. The method has been shown to resolve both high-Z and low-Z materials enclosed in concrete very well. In particular, a tungsten penny with 2 cm radius and 1 cm thickness was clearly visible after no more than 2 weeks of imaging, and a uranium sheet of 0.5 cm thickness was clearly visible with well-defined edges. Furthermore, a novel edge finding method was described, which has been shown to be able to accurately identify the edges of objects embedded in concrete: the size of embedded uranium sheets with 0.5 cm thickness could be reconstructed with a resolution of 1.20 ± 0.37 mm. This method improves the accuracy with which the size and position of an embedded object can be reconstructed beyond the resolution possible in a grid of fixed size, which is of particular use in imaging applications where the precise identification of the size of embedded objects is important, such as the monitoring of uranium corrosion. Future work

includes upgrading the MST prototype system at Bristol to the detector area necessary to image vessels of this size, and then evaluating the method on real data.

Acknowledgement

This work was carried out using the computational facilities of the Advanced Computing Research Centre, University of Bristol - http://www.bris.ac.uk/acrc/.

References

[1] R.C. Ewing et al., *Radiation effects in nuclear waste forms for high-level radioactive waste*, *Progress in nuclear energy*, vol. 29, N. 2, pp.63-127 (1995).

[2] *The Long Term Storage of Radioactive Waste: Safety and Sustainability*, International Atomic Energy Agency (2003).

[3] K. Borozdin et al., *Cosmic-ray muon tomography and its application to the detection of high-Z materials*, *Proceedings of the 46th Annual Meeting, Institute of Nuclear Materials Management, Phoenix, AZ, USA* (2005).

[4] P. Baesso et al., *A high resolution resistive plate chamber tracking system developed for cosmic ray muon tomography*, *JINST*, vol. 8 (2013), N. 8, p. P08006.

[5] P. Baesso et al., *Toward a RPC-based muon tomography system for cargo containers*, *JINST*, vol. 9 (2014), N. 10, p. C10041.

[6] L. J. Schultz et al., *Statistical reconstruction for cosmic ray muon tomography*, *IEEE Transactions on Image Processing*, **16** (2007) 1985.

[7] A. Clarkson et al., *Characterising encapsulated nuclear waste using cosmic-ray muon tomography*, *JINST*, vol. 10 (2015), N. 3, p. P03020.

[8] Eidelman et al., *Review of particle physics*, *Physics Letters B*, vol. 592 (2004), N. 1.

[9] K. Olive et al. (Particle Data Group), *Review of Particle Physics*, *Chin. Phys. C*, **38**, 090001 (2014).

[10] R. Brun and F. Rademakers, *ROOT - An object oriented data analysis framework*, *Nuclear Instruments and Methods in Physics Research*, **A389** (1997) 81.

[11] F. James, M. Roos (CERN), *Minuit: A system for function minimization and analysis of the parameter errors and correlations,* CERN-DD-75-20 (1975), *Comput.Phys.Commun.* 10:343-367,1975.

[12] C. L. Morris et al., *Tomographic imaging with cosmic-ray muons*, *Science and Global Security*, **16** (2008) 37.

[13] C. Thomay et al, *A binned clustering algorithm to detect high-Z material using cosmic muons*, *JINST*, vol. 8 (2013), N. 10, p. P10013.

[14] S. Agostinelli et al., GEANT4 - *A simulation toolkit*, *Nuclear Instruments and Methods in Physics Research*, **A506** (2003) 250.

[15] C. Hagmann, D. Lange and D. Wright, *Cosmic-ray shower generator (CRY) for Monte Carlo transport codes*, in *IEEE Nucl. Sci. Conf. Ser.* **2** (2007) 1143.

[16] Nuclear Decommissioning Authority, *Geological Disposal - Waste Package Specification for 500 litre drum waste packages*, WPSGD No. WPS/300/03, January 2013.